



UNIVERSITY OF LEEDS

This is a repository copy of *Characterisation of carbonated Portland cement paste with optical fibre excitation Raman spectroscopy*.

White Rose Research Online URL for this paper:
<http://eprints.whiterose.ac.uk/110587/>

Version: Accepted Version

Article:

Yue, Y, Wang, JJ, Basheer, PAM orcid.org/0000-0002-0835-8029 et al. (2 more authors)
(2017) Characterisation of carbonated Portland cement paste with optical fibre excitation Raman spectroscopy. *Construction and Building Materials*, 135. pp. 369-376. ISSN 0950-0618

<https://doi.org/10.1016/j.conbuildmat.2017.01.008>

(c) 2017, Elsevier Ltd. This manuscript version is made available under the CC-BY-NC-ND 4.0 license <http://creativecommons.org/licenses/by-nc-nd/4.0/>

Reuse

Unless indicated otherwise, fulltext items are protected by copyright with all rights reserved. The copyright exception in section 29 of the Copyright, Designs and Patents Act 1988 allows the making of a single copy solely for the purpose of non-commercial research or private study within the limits of fair dealing. The publisher or other rights-holder may allow further reproduction and re-use of this version - refer to the White Rose Research Online record for this item. Where records identify the publisher as the copyright holder, users can verify any specific terms of use on the publisher's website.

Takedown

If you consider content in White Rose Research Online to be in breach of UK law, please notify us by emailing eprints@whiterose.ac.uk including the URL of the record and the reason for the withdrawal request.



eprints@whiterose.ac.uk
<https://eprints.whiterose.ac.uk/>

Characterisation of Carbonated Portland Cement Paste with Optical Fibre Excitation Raman Spectroscopy

Yanfei Yue^a, Jing Jing Wang^b, P. A. Muhammed Basheer^c, John J. Boland^b and Yun Bai^{a*}

^aDepartment of Civil, Environmental and Geomatic Engineering, University College London, Gower Street, London, UK, WC1E 6BT

^bCRANN and AMBER Research Centres, Trinity College Dublin, Dublin 2, Dublin, Ireland

^cSchool of Civil Engineering, University of Leeds, Woodhouse Lane, Leeds, UK, LS2 9JT

Abstract

This study demonstrates the potential of developing a future Raman spectroscopy-based sensor system for monitoring carbonation of concrete structures. A tailored optical fibre Raman system was developed under the classical 45 degree geometry with a specific optical fibre assembly acting as the laser excitation-path. This system was then employed to characterise the calcium carbonate polymorphs, i.e. calcite and/or aragonite [ν_1 (CO_3^{2-}) at 1086 cm^{-1}], formed in the carbonated PC paste powder. The finding shows a good potential of optical fibre Raman spectroscopy for monitoring the health condition of concrete structures in the future.

Keywords: Carbonation; Concrete; Durability; Excitation; Optical Fibre; Raman spectroscopy; Structural Health Monitoring.

1. INTRODUCTION

In recent decades, structural health monitoring (SHM) with the employment of sensors has shown some success in monitoring the physical properties, such as stress and strain, of concrete structures [1, 2]. However, it has been increasingly recognised that, instead of physical properties, monitoring the changes in the chemical composition of hardened cement paste in concrete is more important because this can provide an in-depth understanding on the evolution of concrete deterioration mechanisms such as chloride ingress, carbonation and sulphate attack over time, so that both the prediction of service life and the diagnosis of the

*Corresponding author: Dr. Yun Bai. Email address: yun.bai@ucl.ac.uk. Tel: +44(0)20 76792386. Fax: +44(0)20 76793042

Postal address: Department of Civil, Environmental & Geomatic Engineering, Chadwick Building, Gower Street, London, WC1E 6BT, UK

causes of deterioration can be established. Although electrical sensor (ES) [3, 4] and fibre optic sensor (FOS) [5-7] have been attempted to monitor the deterioration mechanisms of concrete structures, the electrical change of ES can also be attributed to some other factors such as the humidity change or the change of the microstructure of cement matrix due to continued hydration [8]. Therefore, ES cannot clearly differentiate each individual deterioration mechanism. On the other hand, even though FOS can overcome the issues facing ES by impregnating the fibre with specific chemical dyes so that the colour variation induced by the deterioration mechanisms can be identified and, even, quantified, it responds irreversibly and cannot survive the inherently harsh alkaline environment of concrete for long time [9].

In contrast, under the fingerprint characterisation capacity of Raman spectroscopy [10, 11], the reaction products of various deterioration mechanisms, such as calcium carbonate polymorphs (e.g., calcite, vaterite and aragonite) [12-19] from carbonation and sulphate-bearing products (i.e., gypsum, ettringite and thaumasite) [20-23] from sulphate attack, can be clearly differentiated by their unique vibration bands (wavenumber in cm^{-1}) and this can effectively overcome the limitations of ES. Moreover, as Raman spectroscopy works on the principle of intrinsic vibration of molecules, the chemical dyes as employed in the FOS is no longer needed which can totally eliminate the long-term instability and irreversibility issues facing FOS. On the other side of the spectrum, in recent years, the application of optical fibre assemblies, especially the low-loss optical fibre, has also enhanced the long-distance remote signal-collection capability of optical fibre Raman system [24-27]. Therefore, remote monitoring with optical fibre Raman system is becoming a reality. Surprisingly, up to date, the application of optical fibre Raman system in monitoring the durability of concrete structure has not been attempted in the literature. Previous study carried out by the authors showed that there is a good potential to monitor sulphate attack with optical fibre Raman spectroscopy [7]. This paper, therefore, extends the previous work to explore the potential of using optical fibre Raman system to monitor the carbonation mechanism of concrete.

Among various durability issues facing structural concrete, carbonation is one of the two primary deterioration mechanisms leading to the corrosion of reinforcements. It is a chemical reaction between the CO_3^{2-} (i.e., carbon dioxide must be dissolved in concrete pore solution first) and the Ca-bearing phases in the cement matrix. Whilst virtually all the hydration products (i.e. calcium hydroxide, calcium silicate hydrate and various calcium aluminate or ferro-aluminate hydrates) can react with CO_2 to produce calcium carbonate, silica gel and hydrated aluminium and iron oxides, the dominant reaction is the one between calcium hydroxide [$\text{Ca}(\text{OH})_2$] and CO_2 which converts $\text{Ca}(\text{OH})_2$ to calcium carbonate (CaCO_3), leading to a

reduction in the pH of concrete pore solution and subsequent corrosion of reinforcing bars [28, 29]. The calcium carbonate thus formed mainly exists in the form of three crystallised polymorphs, namely, calcite (well-crystallised stable phase) and vaterite & aragonite (crystallised meta-stable phases) [12, 30, 31]. Previous research reported in the literature on characterising carbonation products with bench-mounted Raman spectroscopy (i.e. no fibre optical assemblies were employed) indicates that the four internal vibration modes of CO_3^{2-} , namely ν_1 (symmetric stretching), ν_2 (out-of-plane bending) (very weak), ν_3 (asymmetric stretching) and ν_4 (in-plane bending), together with the Ca-O lattice vibration (LV), all can be identified [12-19]. Table 1 summarises the Raman bands and their related assignments of these three crystallised calcium carbonates from the literature. It can be seen that, in addition to the wavenumber shifts between these three polymorphs, each individual calcium carbonate polymorph can be readily differentiated by their unique Raman features as outlined below:

- i) Degeneration of the ν_1 symmetric stretching (CO_3^{2-}) band of vaterite vs non-degeneration of the ν_1 (CO_3^{2-}) bands of calcite and aragonite (i.e. double peaks vs single peak). This feature can clearly differentiate vaterite from calcite and aragonite.
- ii) Degeneration of the ν_3 asymmetric stretching (CO_3^{2-})/ ν_4 in-plane bending (CO_3^{2-}) mode of vaterite and aragonite vs non-degeneration of the ν_3/ν_4 (CO_3^{2-}) modes of calcite (i.e. multiple peaks vs single peak). This can differentiate calcite from aragonite and vaterite.

Table 1. Assignment of Raman bands of calcium carbonate polymorphs [12-19]

| | Lattice vibration | ν_1 symmetric stretching of CO_3^{2-} | ν_2 out-of-plane bending of CO_3^{2-} | ν_3 asymmetric stretching of CO_3^{2-} | ν_4 in-plane bending of CO_3^{2-} |
|------------------|--|---|---|--|---|
| Calcite | 154, 281 | 1085 | | 1434 | 711 |
| Aragonite | 143, 153, 180, 190, 206, 247, 261, 284 | 1085 | 853 | 1462, 1574 | 701, 705 |
| Vaterite | 267, 300, 325 | 1074, 1090 | 874 | 1445, 1485 1550, 1595 | 668, 682 740, 750 |

Therefore, the combination of the Raman spectroscopy with the latest advancement in optical fibre technique offers a unique opportunity to monitor the chemistry evolution during the carbonation of concrete structures. To verify this feasibility, in the current study, a tailored

Raman spectroscopy with optical fibre excitation pathway was developed and employed to characterise the carbonated Portland cement (PC) paste powder. Bench-mounted Raman spectroscopy and X-ray Diffraction (XRD) analyses on the carbonated PC paste powder were also conducted to verify the results obtained from the optical fibre Raman system.

2. MATERIAL AND METHODS

2.1 Sample preparation

2.1.1 Materials

Portland cement (PC) used in this study was 42.5R CEM I (in accordance with BS EN 197-1:2011) supplied by QUINN Group and its chemical composition is given in Table 2. The chemical reagent calcium carbonate (main phase is calcite with an assay >98%) was purchased from the Fisher Scientific (UK) which was used as a pure calcium carbonate in the following characterisation.

Table 2. Chemical composition of Portland cement

| Oxides | SiO ₂ | Al ₂ O ₃ | Fe ₂ O ₃ | CaO | MgO | K ₂ O | Na ₂ O | SO ₃ |
|--------|------------------|--------------------------------|--------------------------------|-------|------|------------------|-------------------|-----------------|
| % wt | 23.00 | 6.15 | 2.95 | 61.30 | 1.80 | 0.68 | 0.22 | 2.50 |

2.1.2 Manufacture and carbonation of PC paste

The cement paste was manufactured with a water-to-cement ratio (W/C) of 0.35 using a Hobart planetary mixer, cast in plastic centrifugal tubes and vibrated for around 1 minute to remove the air bubbles. After 24-hour initial curing in centrifugal tubes at 20 ± 1 °C, the specimens were removed from the tubes and covered with water saturated hessian and then sealed in plastic sample bags. These bags were then stored in a curing room at constant temperature of 20 ± 1 °C for around 6 months. The wet hessian was regularly checked and replaced once the moisture level was low. At the end of six months, selected pastes were first ground into powders (with fineness of 63 μ m) prior to being exposed to carbonation. The powders were then subjected to accelerated carbonation environments (temperature of 20 ± 1 °C, relative humidity of $60 \pm 5\%$ and CO₂ concentration of $5 \pm 0.5\%$) in a LEEC carbonation chamber for 14 days, in an attempt to obtain extensively carbonated samples. The powders were then used for the Raman spectroscopy study and XRD analyses below.

2.2 Bench-mounted Raman spectroscopy

The bench-mounted Raman spectrometer used in this study was a Renishaw inVia microscope equipped with a Charged Coupled Device (CCD) detector. It works under the back-scattering geometry with the laser beam being focused into a laser-spot of about 1.26 μm diameter by means of an objective with 50X magnification and numerical aperture (N.A.) of 0.5 before interrogating the sample. A 514.5 nm single-line Argon-ions laser with output power of 25.5 mW was employed as the excitation source. The measured power at the sampling level was about 4.1 mW, with most of the laser lost during transmitting/reflecting through the excitation optics. Prior to each experiment, the Raman shift was calibrated using the well-defined peak of silicon wafer at about 520 cm^{-1} . After calibration, Raman spectra were recorded with exposure time of 10 seconds and accumulations of 10 to improve the signal-to-noise ratio (SNR). In this study, the bench-mounted Raman analysis was carried out to verify the results obtained from the optical fibre Raman analysis.

2.3 Optical fibre excitation Raman spectroscopy

The previous work carried out by the authors [7] has established successfully a fibre optic Raman system with a 45 degree 'fibre excitation + objective collection' geometry, which is capable of laser illumination, laser excitation and signal collection. Building upon this, the current study employed an optical fibre excitation pathway with the same optical geometry, but different laser source (i.e., 514.5 nm) and built-in optics (e.g., bandpass filter), to identify the carbonation mechanisms in cementitious materials. Furthermore, in order to compare the laser power densities between these bench-mounted Raman spectrometer and the newly developed optical fibre Raman system, the laser power in these two optical sub-paths were measured at the laser focusing point and are reported in Table 3. In the bench-mounted Raman spectroscopy, the laser interrogated the sample with a measured power of 4.1 mW which corresponded to a 16% coupling efficiency as the out-put laser of 25.5 mW. In contrast, a much higher excitation laser power level, 18.1 mW, was measured in the fibre excitation pathway which represented a 71% coupling efficiency. However, due to the fact that the focused laser spot size of the optical fibre Raman system ($50.0\ \mu\text{m}^2$) was much larger than that of the bench-mounted Raman spectroscopy ($1.2\ \mu\text{m}^2$), i.e., nearly 42 times larger, the calculated power density (i.e. power-to-excitation spot area) of the optical fibre Raman system ($0.4\ \text{mW}/\mu\text{m}^2$) was much lower than that of the bench mounted Raman spectroscopy ($3.4\ \text{mW}/\mu\text{m}^2$).

Table 3. Laser powers and densities at exciting points of both Raman systems

| | Excitation laser power | Excitation laser spot area | Excitation laser power density |
|--|---------------------------|-------------------------------|-----------------------------------|
| Optical fibre excitation Raman system | 18.1 mW | 50.0 μm^2 | 0.4 mW/ μm^2 |
| Bench-mounted Raman system | 4.1 mW | 1.2 μm^2 | 3.4 mW/ μm^2 |

2.4 Raman Data Process

2.4.1 Peak fitting

The peaks identified in the Raman spectra are usually fitted under appropriate logarithm functions in order to retrieve the genuine Raman features. In this study, baseline correction was first employed to subtract the background in the Raman spectra. Then, Lorentz function, which is accepted as an appropriate fitting function for crystallised phases, was adopted to fit the Raman peaks [32]. Under the Lorentz function, four features of a particular peak can be obtained, namely, wavenumber, height, area and FWHM (full width at half maximum), which can be illustrated as follows:

- i) Wavenumber (X_c , cm^{-1}) – the Raman shift of certain ionic groups;
- ii) Height (H) – the intensity of the peak above the corrected baseline;
- iii) Area (A) – the integrated area of the peak above the corrected baseline;
- iv) FWHM (W , cm^{-1}) – the full width at half maximum of the peak.

These four Raman peak features indicate distinct information about the analytes. The wavenumber of the Raman peak is the fingerprint used to distinguish materials – as each ionic group has its own unique wavenumber under laser excitation [10]. FWHM is considered to be relevant to the crystallisation degree of the analytes [33], i.e., its enlargement would suggest the weakening of the crystallisation. On the other hand, the other two features, i.e., peak height and peak area, are both related to the quantitative information of the analytes [34]. In this study, the Raman shift (wavenumber of the Raman peaks) retrieved were employed to identify the type of the products formed, and the height of the peaks were used for calculating the signal-to-noise ratio (SNR) of the spectra (detailed in Section 2.4.2), respectively. The peak analysis of all the spectra was conducted with the Origin-Pro 8.6 (USA).

2.4.2 Calculation of signal-to-noise ratio (SNR)

The signal-to-noise ratio (SNR) is one of the most significant parameters of the Raman spectra, which indicates the quality of the spectra. In the current study, the SNR was employed to quantitatively compare the spectrum obtained from the optical fibre Raman spectroscopy with that from the bench-mounted Raman spectroscopy. This information was then used to identify the advantages and disadvantages of the newly established optical fibre Raman system. In this study, the SNR values were calculated according to the method specified in ASTM E579-04 [35], as follows:

$$SNR = \frac{\text{Signal level}}{\text{Noise (RMS) level}} \quad (1)$$

Where, the signal level is the peak intensity after subtracting the background;

the noise level is obtained by root mean square (RMS) method, which is the standard deviation of the intensity values of a selected Raman shift region on the spectrum after subtracting the background.

2.5 X-ray Diffraction (XRD)

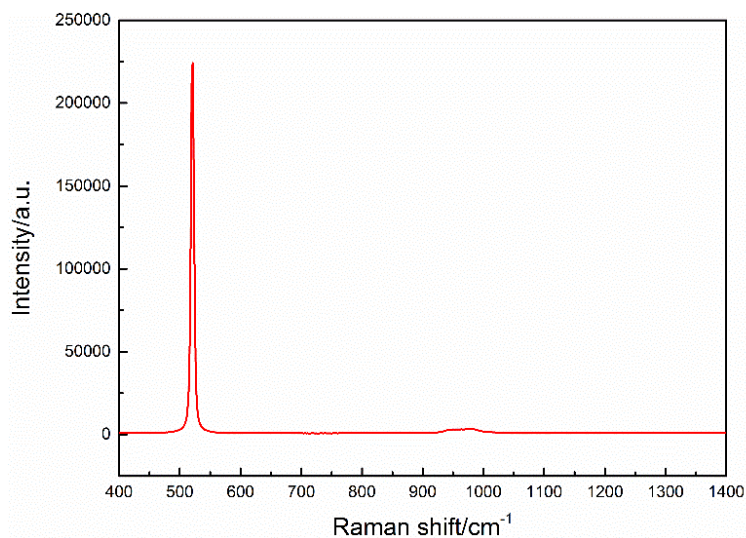
The powder method of X-ray diffraction was adopted in the present study as a supplementary technique to validate the results obtained from both Raman systems. An XPERT-PRO diffractometer with an X-ray source of Co K α radiation ($\lambda=1.78901 \text{ \AA}$) was used. A scanning speed of 2 °/min and step size of 0.017° 2 θ were used to examine the samples in the range of 5° to 65° 2 θ . The X-ray tube voltage and current were fixed at 40 kV and 30 mA, respectively.

3. RESULTS AND DISCUSSION

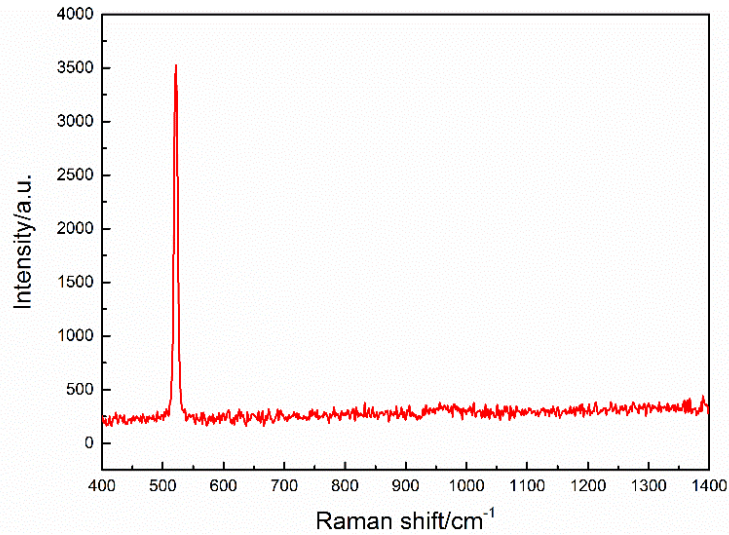
3.1 Calibration of Raman spectroscopy (with/without optical fibre)

Calibration of Raman spectroscopy can be considered as a process to relate the observed spectra frequencies to their true values by adjusting the instrument [11]. In the case of optical fibre Raman system, this could also include optics alignment and initial optimisation. In the current study, the bench-mounted Raman and optical fibre Raman systems were calibrated through the same methodology as the previous work [7] by using the well-defined Raman peak of silicon wafer at $520.2 \pm 0.5 \text{ cm}^{-1}$ [36]. Figs. 1(a) and 1(b) present the Raman spectra of the

silicon wafer collected under bench-mounted Raman and optical fibre Raman systems respectively. In Fig. 1 the Raman fingerprint peaks of silicon were successfully retrieved by both these two Raman systems as evidenced by an intense and sharp peak at 521 cm^{-1} , indicating that these two optical systems were fully calibrated. The signal-to-noise (SNR) ratios of the silicon peak were then calculated according to the method described in Section 2.4.2 (ASTM E579-04) [35]. The corresponding results, along with the wavenumber of the peak retrieved, are presented in Table 4. Apparently, the intensity of the silicon peaks obtained from these two Raman systems were dramatically different, i.e., 3659.0 from optical fibre excitation Raman system, which was much lower than that of 251934.7 from bench-mounted Raman spectroscopy – only about 1.5%. The noise level under fibre mode (32.2) was lower than that of bench-mounted Raman spectroscopy (88.6) as well. However, due to the huge difference in the signal intensities between these two Raman systems, even though the noise level of the fibre mode was relatively lower, the overall SNR of the Raman spectra collected under the optical fibre excitation Raman system (113.6) was still much lower than that of the bench-mounted Raman spectroscopy (2843.5), i.e., around 25 times lower. As discussed, these differences in the Raman spectra features can be explained mainly by two factors, i.e., the lower power density hence lower excitation efficiency of the optical fibre Raman system, as well as lower signal collection efficiency (45 degree) of fibre pathway compared to bench-mounted Raman spectroscopy (backscattering).



(a) Bench-mounted Raman



(b) Optical fibre Raman

Fig.1 Raman spectra of silicon wafer

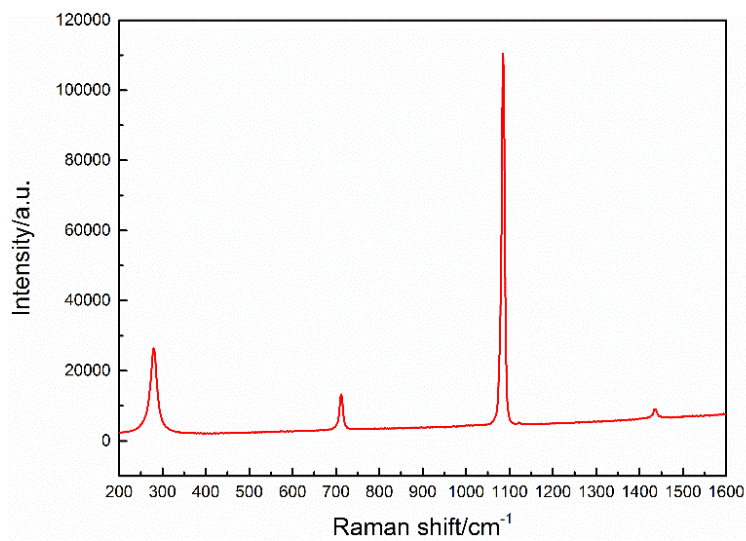
Table 4. Wavenumber and SNR of silicon peak at 521 cm⁻¹

| | Wavenumber | Signal intensity | Noise level | SNR |
|--|----------------------|-------------------------|--------------------|------------|
| Bench-mounted Raman system | 521 cm ⁻¹ | 251934.7 | 88.6 | 2843.5 |
| Optical fibre excitation Raman system | 521 cm ⁻¹ | 3659.0 | 32.2 | 113.6 |

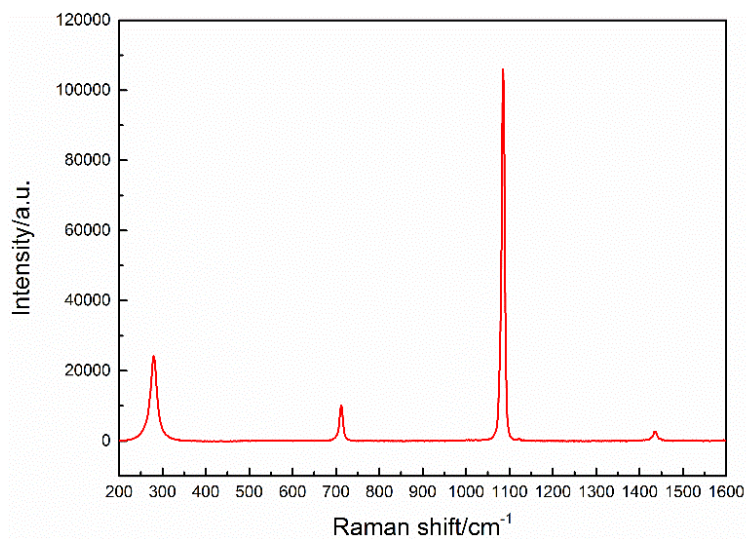
3.2 Characterisation of pure calcium carbonate with Raman spectroscopy (with/without optical fibre)

Calcium carbonate is the principal product formed in the carbonated cementitious materials. Amongst the various calcium carbonate polymorphs, calcite is the most stable form at ordinary temperature and pressure [37]. Hence, in the current study, the pure calcium carbonate (calcite) was used as a reference and characterised first by bench-mounted Raman and optical fibre Raman systems. The Raman spectra collected were then used as bench-mark information for the subsequent Raman spectroscopy analysis of the carbonated Portland cement (PC) paste powder in the next section. The Raman spectra of the calcite so obtained are presented in Fig. 2 (without fibre) and Fig. 3 (with fibre), respectively.

As shown in Fig. 2(b), the bench-mounted Raman spectrum of calcite was dominated by a sharp peak located at 1085 cm^{-1} , which is attributed to the ν_1 symmetric stretching band of CO_3^{2-} in calcite. In addition, three minor bands were also identified at 280 cm^{-1} , 712 cm^{-1} and 1436 cm^{-1} , which can be assigned to the Ca-O lattice vibration (Ca-O LV), the ν_4 in-plane bending mode and the ν_3 asymmetric stretching vibration in calcite, respectively. In Fig. 3(b), the Raman signal of calcite was also successfully retrieved by optical fibre excitation Raman system as evidenced by a sharp and intense peak at 1086 cm^{-1} ($\nu_1\text{ CO}_3^{2-}$), a prominent peak at 280 cm^{-1} (Ca-O LV) and two weak peaks located at 712 cm^{-1} ($\nu_4\text{ CO}_3^{2-}$) and 1437 cm^{-1} ($\nu_3\text{ CO}_3^{2-}$), respectively.

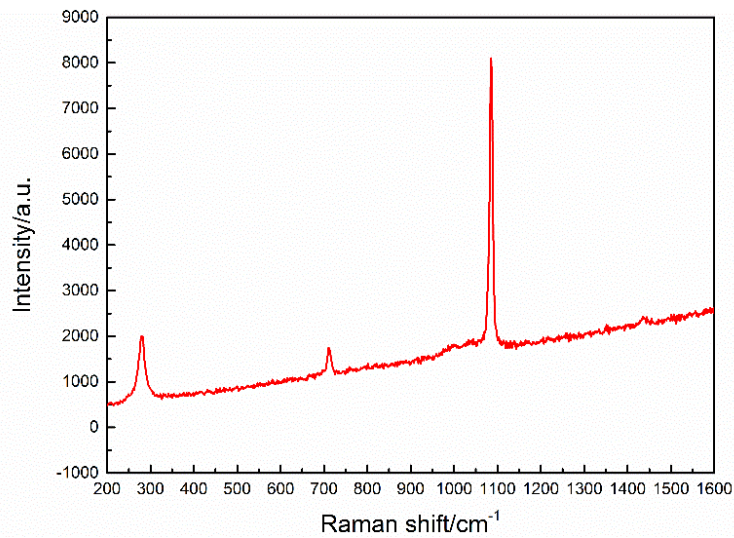


(a) Original spectrum

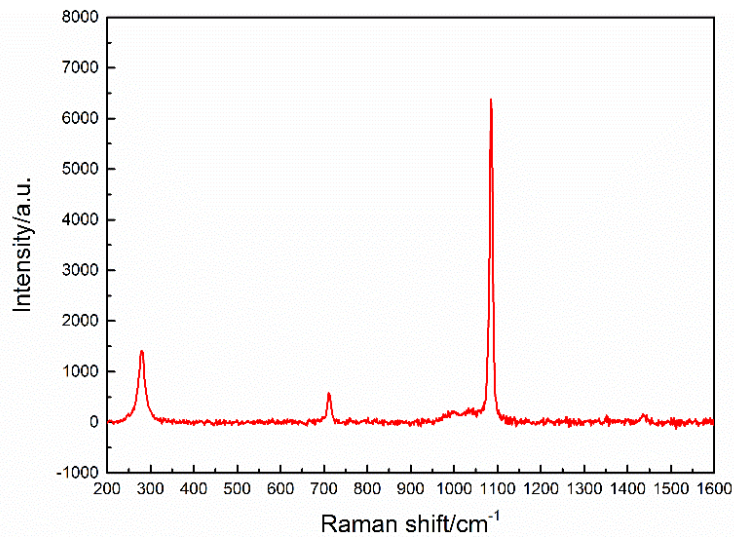


(b) Spectrum after subtracting background

Fig.2 Bench-mounted Raman spectra of calcite



(a) Original spectrum



(b) Spectrum after subtracting background

Fig.3 Optical fibre Raman spectra of calcite

Table 5 summarises all the identified Raman bands and the related assignments of the Raman spectra shown in Fig. 2 (bench-mounted Raman spectroscopy) and Fig. 3 (fibre Raman system). Furthermore, the most intense peak ($\nu_1 \text{CO}_3^{2-}$) was selected as reference and its SNR under these two optical systems were calculated and reported in Table 6. In Table 5, all the fingerprint bands identified from optical fibre Raman system are in good agreement with those from bench-mounted Raman spectroscopy, indicating that the optical fibre Raman spectroscopy is adequate to differentiate calcite. On the other hand, as shown in Table 6, the SNR of the $\nu_1 \text{CO}_3^{2-}$ under optical fibre excitation Raman system was lower than that of the bench-mounted Raman spectroscopy. This finding of calcite is consistent with that of silicon (Section 3.1), which again could be attributed to the lower power density and less efficient collection geometry of the optical fibre excitation Raman system.

Table 5. Raman bands and assignments of calcite

| | Bench-mounted Raman system | Optical fibre excitation Raman system | Assignments |
|--------------|---------------------------------------|--|---|
| | 1085 cm ⁻¹ | 1086 cm ⁻¹ | Symmetric stretching (ν_1) of CO ₃ ²⁻ in calcite |
| Raman | 1436 cm ⁻¹ | 1437 cm ⁻¹ | Asymmetric stretching (ν_3) of CO ₃ ²⁻ in calcite |
| shift | 712 cm ⁻¹ | 712 cm ⁻¹ | In-plane bending (ν_4) of CO ₃ ²⁻ in calcite |
| | 280 cm ⁻¹ | 280 cm ⁻¹ | Lattice vibration (LV) in calcite |

Table 6. Wavenumber and SNR of ν_1 CO₃ in calcite

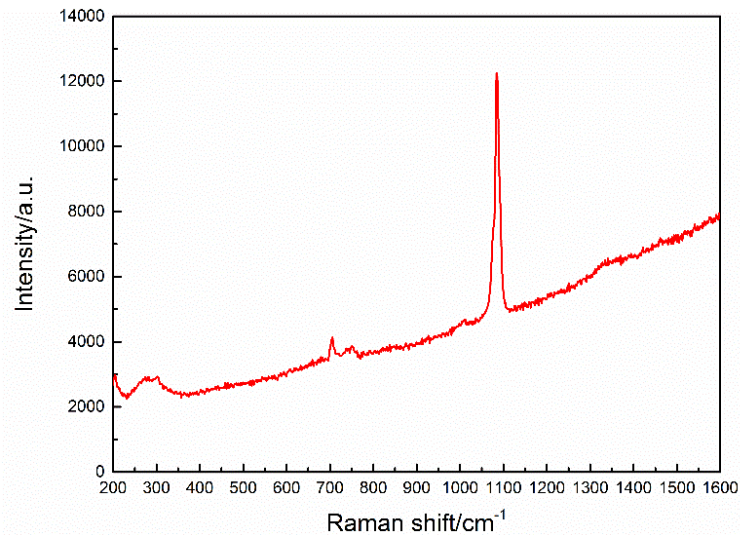
| | Wavenumber | Signal intensity | Noise level | SNR |
|--|-----------------------|-----------------------------|------------------------|------------|
| Bench-mounted Raman system | 1085 cm ⁻¹ | 112612.1 | 73.6 | 1530.1 |
| Optical fibre excitation Raman system | 1086 cm ⁻¹ | 6627.4 | 35.3 | 187.7 |

3.3 Characterisation of carbonated PC paste powder with Raman spectroscopy (with/without optical fibre)

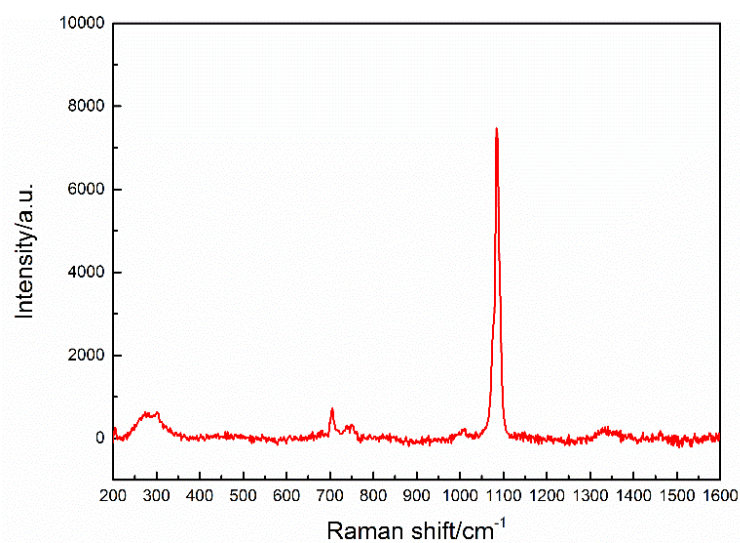
In cementitious materials, the intruded CO₂ is chemically bound by cement hydrates as CaCO₃, which precipitates in various forms including calcite (well-crystallised/stable), vaterite and aragonite (poorly-crystallised/metastable). While the pure calcite has been successfully identified under both bench-mounted Raman and optical fibre excitation Raman systems in Section 3.2, the characterisation of calcium carbonate formed in the carbonated PC system could potentially be difficult owing to the following two reasons:

- i) Heterogeneous nature of cementitious materials. Due to the heterogeneous nature of the hydration products formed in hardened cement matrix, it is highly unlikely that the calcium carbonate formed in the carbonated cement sample can be uniformly distributed and it is hence potentially difficult for Raman spectroscopy to identify – as the excitation spot of Raman spectroscopy is only confined to few micron meters.
- ii) The impurities existing in the cement (e.g. organic compounds like grinding agent), the defects introduced during grinding and the inter-particle scattering could all cause strong background to the intrinsically weak Raman peaks [38].

Hence, similar to the characterisation of pure calcite reported in the previous section, in order to identify the feasibility of characterising the calcium carbonate formed in carbonated cementitious matrix with optical fibre excitation Raman system, bench-mounted Raman analysis was first carried out as a benchmark and the Raman spectra obtained are shown in Fig. 4.



(a) Original spectrum

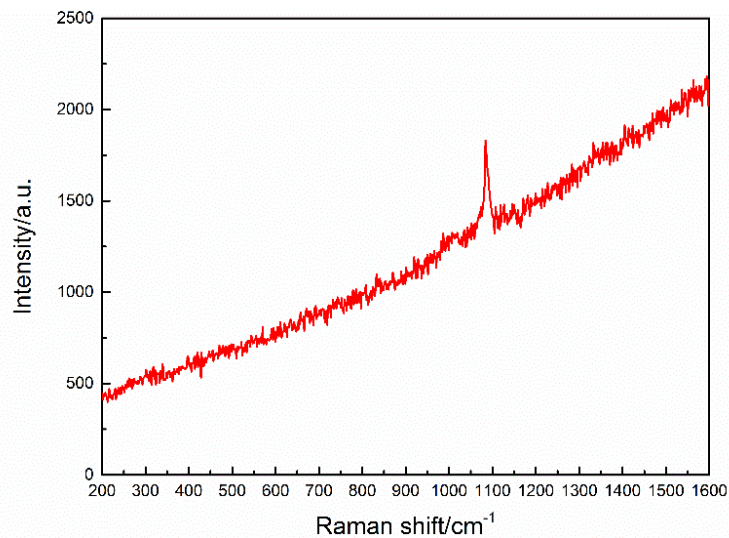


(b) Spectrum after subtracting background

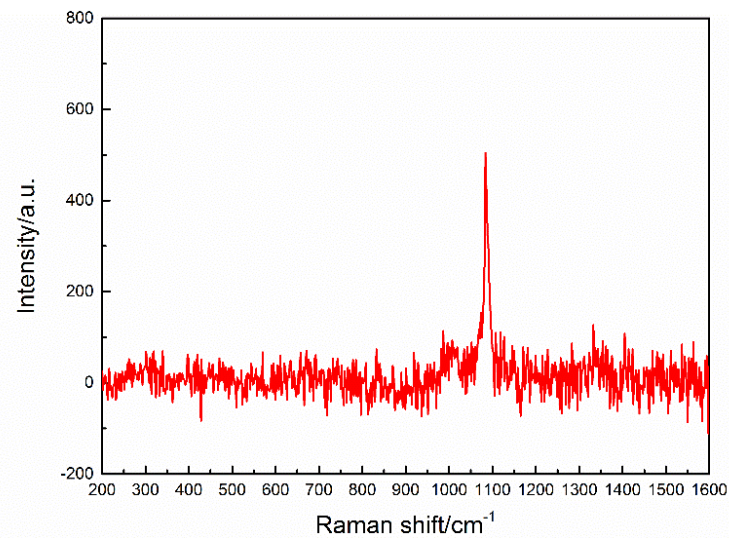
Fig. 4 Bench-mounted Raman spectra of the carbonated PC paste powder

In Fig. 4(a), as expected, strong sloping background was observed in the Raman spectrum of carbonated PC paste powder. This could potentially be attributed to, as aforementioned, the organic contaminants in cement, the inter-particle scattering and the defects caused by grinding during cement manufacture [38]. The spectrum after subtracting the background is presented in Fig. 4(b). The most intense peak located at 1085 cm⁻¹ is again the ν_1 symmetric

stretching band of the CO_3^{2-} in calcite and/or aragonite, and the humps located at about $268/300\text{ cm}^{-1}$ is the LV mode of the Ca-O bond in vaterite. Furthermore, some minor bands were identified at 705 cm^{-1} and $738/751\text{ cm}^{-1}$. The former is the ν_4 in-plane bending mode of the CO_3^{2-} in calcite and the latter is the ν_4 mode in vaterite. Obviously, the carbonated PC paste powder demonstrated severe carbonation as manifested by these pronounced Raman features of calcite and/or aragonite and vaterite. More importantly, it is worth highlighting that all these features have been successfully identified by the bench-mounted Raman spectroscopy. Following this bench-mounted Raman analysis, the same carbonated PC paste sample was then analysed by the optical fibre excitation Raman system and the Raman spectra are shown in Fig. 5.



(a) Original spectrum



(b) Spectrum after subtracting background

Fig. 5 Optical fibre Raman spectra of the carbonated PC paste powder

Compared to Fig. 4(a), the original spectrum in Fig. 5(a) showed an even stronger sloping background. In addition to the organic compounds, the inter-particle scattering and the defects caused by grinding during cement manufacture as discussed under bench-mounted results, additional contribution could also come from the optical fibre. In an attempt to eliminate these effects, baseline correction was also employed to subtract the background and the new spectrum is shown in Fig. 5(b). As can be seen, the spectrum in Fig. 5(b) was also dominated by a sharp peak located at 1086 cm^{-1} , which is again due to the ν_1 symmetric stretching band of the CO_3^{2-} in calcite and/or aragonite. It should be noted that, compared to the spectrum obtained under bench-mounted Raman spectroscopy, other Raman features such as the LV mode of the Ca-O bond in vaterite, ν_4 in-plane bending mode of the CO_3^{2-} in calcite and the ν_4 mode in vaterite, have not been observed under optical fibre system. This could have been caused by the heterogeneous nature of the cementitious materials. Future study is, thus, still needed in order to overcome this. Nonetheless, as the ν_1 band is the most important vibrational mode for identifying carbonation mechanism, the current results suggest that optical fibre Raman system is sufficient and sensitive in differentiating carbonation mechanisms in carbonated PC paste which clearly demonstrates a potential for developing a Raman spectroscopy based optical fibre sensor system for monitoring the carbonation progress in concrete structures in the future.

To further compare the working capacity of these two Raman systems for characterising cementitious materials, all the bands identified by the bench-mounted Raman and the optical fibre Raman systems are summarised in Table 7, whereas the wavenumber and SNR of the ν_1 CO_3^{2-} peak are compared in Table 8.

Table 7. Raman bands and assignments of the carbonated PC paste powder

| | Bench-mounted Raman system | Optical fibre excitation Raman system | Assignments |
|------------------------|---------------------------------------|--|---|
| | 1085 cm^{-1} | 1086 cm^{-1} | Symmetric stretching (ν_1) of CO_3^{2-} in calcite/aragonite |
| Raman shift | 705 cm^{-1} | | In-plane bending (ν_4) of CO_3^{2-} in calcite |
| | $738/751\text{ cm}^{-1}$ | | In-plane bending (ν_4) of CO_3^{2-} in vaterite |
| | $268/300\text{ cm}^{-1}$ | | Lattice vibration (LV) in vaterite |

Table 8. Wavenumber and SNR of ν_1 CO_3^{2-} in the carbonated PC paste powder

| | Wavenumber | Signal intensity | Noise level | SNR |
|--|-----------------------|------------------|-------------|-------|
| Bench-mounted Raman system | 1085 cm^{-1} | 7578.4 | 54.0 | 140.3 |
| Optical fibre excitation Raman system | 1086 cm^{-1} | 420.3 | 31.0 | 13.6 |

From Table 7 and Table 8, the following features can be observed:

- i) Different vibration modes were identified under bench-mounted Raman and optical fibre excitation Raman systems. Under the bench-mounted Raman spectroscopy, the ν_1 symmetric stretching band of the CO_3^{2-} , ν_4 in-plane bending mode and LV mode were successfully identified. However, only ν_1 symmetric stretching band of CO_3^{2-} was identified under the optical fibre excitation Raman system due to the heterogeneous nature of the cementitious materials.
- ii) Different signal intensity, noise level and overall SNR were identified under the bench-mounted Raman and the optical fibre excitation Raman systems. As can be seen from Table 8, the signal intensity of the ν_1 CO_3^{2-} peak under the bench-mounted Raman spectroscopy was much higher than that of the optical fibre excitation Raman system, i.e., 7578.4 vs 420.3. The same phenomenon was observed in the noise level, i.e., 31.0 of fibre mode vs 54.0 of bench-mounted Raman. Accordingly, different SNRs were achieved under the bench-mounted Raman spectroscopy (140.3) and the optical fibre excitation Raman system (13.6). As indicated in Section 3.1, this could be caused by the lower power density and the less efficient collection geometry of the optical fibre excitation Raman system as compared with the bench-mounted Raman spectroscopy.

3.4 X-ray diffraction analysis on carbonated PC paste powder

In this study, XRD analysis was carried out on the carbonated cement sample in order to verify the calcium carbonate polymorphs formed during the carbonation process. This can, subsequently, also be used to verify the results obtained from both the Raman systems. The XRD pattern of the carbonated PC paste powder is shown in Fig. 6. Obviously, several peaks of the calcium carbonate crystallised phases formed in the carbonated PC paste powder have been clearly identified, i.e. $2\theta = 26.8^\circ$, 34.3° & 46.1° for calcite, $2\theta = 24.5^\circ$, 29.0° & 31.5° for vaterite and $2\theta = 30.6^\circ$, 36.2° & 48.4° for aragonite. Hence, it is apparent that different calcium

carbonate polymorphs were formed during the accelerated carbonation and dominate the composition of the PC paste sample analysed. Additionally, various cement hydration products have also been recognised, such as portlandite ($2\theta = 21.0^\circ, 33.5^\circ$ & 39.8°).

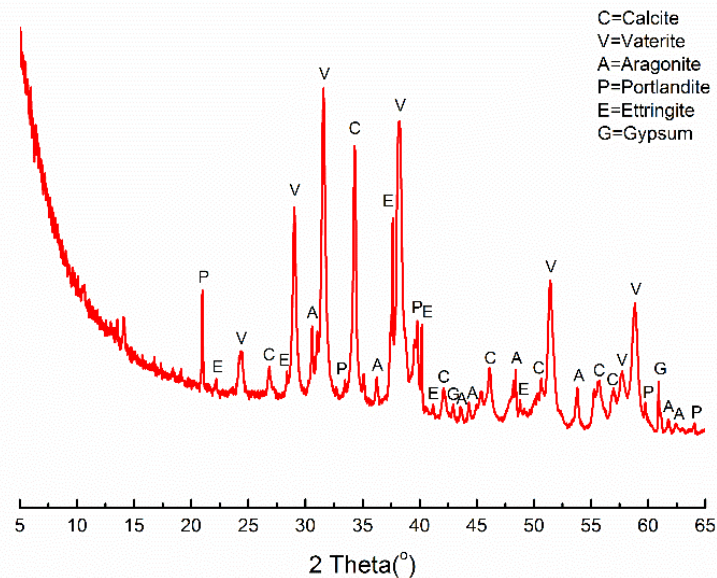


Fig.6 XRD pattern of the carbonated PC paste powder

4. CONCLUSIONS

In the current study, a tailored optical fibre excitation Raman system with a 514.5 nm excitation laser under a 45 degree geometry of ‘optical fibre excitation + spectrometer objective collection’ was successfully developed and employed to characterise the calcium carbonate polymorphs formed in a carbonated Portland cement (PC) paste powder. Under this optical fibre excitation Raman system, the calcite and/or aragonite [ν_1 (CO_3^{2-}) at 1086 cm^{-1}] formed in the carbonated PC paste sample were clearly identified and differentiated, with the results being well verified by the bench-mounted Raman spectroscopy and XRD analyses. The results indicate that optical fibre Raman spectroscopy is adequate to differentiate calcium carbonate polymorphs formed in the carbonated cementitious materials, therefore, there is a great potential for developing a Raman spectroscopy based optical fibre sensor system capable of monitoring the evolution of carbonation in concrete structures in the future. However, it was the powder of hardened cement paste which had been used to verify the concept of optical fibre Raman spectroscopy in this study. Before this system could be embedded in concrete as a sensor, suitable packaging techniques still need to be developed in order to protect the sophisticated optical components in the severe alkaline environment of

concrete. Furthermore, the relatively low SNR of the Raman spectra obtained from optical fibre Raman system also needs to be addressed in the future.

ACKNOWLEDGEMENTS

This research was partially funded by the QualityNano Transnational Access grant and UK Royal Society International Exchange Scheme with Ireland (IE131481). The authors would also like to acknowledge the support received from the EPSRC UK-China Science Bridge project (EP/G042594/1), China Scholarship Council and Faculty of Engineering Sciences at UCL which enabled Dr Yanfei Yue to finish her PhD at UCL. The CEM I Portland cement used in this research was supplied by QUINN Group.

REFERENCES

- [1] A.A. Mufti, G. Tadros, P.R. Jones, Field assessment of fibre-optic bragg grating strain sensors in the Confederation Bridge, *Can. J. Civil. Eng.* 24(6) (1997) 963-966.
- [2] S. Liehr, P. Lenke, M. Wendt, K. Krebber, M. Seeger, E. Thiele, H. Metschies, B. Gebreselassie, J.C. Munich, Polymer optical fiber sensors for distributed strain measurement and application in structural health monitoring, *IEEE Sens. J.* 9(11) (2009) 1330-1338.
- [3] W. McCarter, M. Emerson, H. Ezirim, Properties of concrete in the cover zone: developments in monitoring techniques, *Mag. Concrete. Res.* 47(172) (1995) 243-251.
- [4] M. Raupach, P. Schießl, Macrocell sensor systems for monitoring of the corrosion risk of the reinforcement in concrete structures, *NDT & E. Int.* 34(6) (2001) 435-442.
- [5] D.O. McPolin, P. Basheer, A.E. Long, W. Xie, T. Sun, K.T. Grattan, Development and longer term in situ evaluation of fiber-optic sensors for monitoring of structural concrete, *IEEE Sens. J.* 9(11) (2009) 1537-1545.
- [6] M.P. Basheer, K.T.V. Grattan, T. Sun, A.E. Long, D. McPolin, W. Xie, Fiber optic chemical sensor systems for monitoring pH changes in concrete, *Proc. SPIE* 5586. (2004)144-153.
- [7] Y. Yue, Y. Bai, P.M. Basheer, J.J. Boland, J.J. Wang, Monitoring the cementitious materials subjected to sulfate attack with optical fiber excitation Raman spectroscopy, *Opt. Eng.* 52(10) (2013) 104107-104107.
- [8] P.A.M. Basheer, S. Srinivasan, S. Nanukuttan, D. Cleland, Smart and Green Structural and Repair Materials, Technical Report TR 6.4, Smart structural materials with permanent monitoring system for concrete: Novel sensors for monitoring the durability of concrete structures, 2012, Atlantic Area Translational Programme.

- [9] R.D. Davies, N.R. Buenfeld, Automated monitoring of the deterioration of concrete structures, Department of Trade and Industry, London, 2007.
- [10] D.A. Long, Raman spectroscopy, McGraw-Hill International Book Company, New York, 1977.
- [11] R.L. McCreery, Raman spectroscopy for chemical analysis, John Wiley & Sons, New York, 2000.
- [12] S. Martinez-Ramirez, S. Sanchez-Cortes, J. Garcia-Ramos, C. Domingo, C. Fortes, M. Blanco-Varela, Micro-Raman spectroscopy applied to depth profiles of carbonates formed in lime mortar, *Cement. Concrete. Res.* 33(12) (2003) 2063-2068.
- [13] C. Gabrielli, R. Jaouhari, S. Joiret, G. Maurin, In situ Raman spectroscopy applied to electrochemical scaling. Determination of the structure of vaterite, *J. Raman. Spectrosc.* 31(6) (2000) 497-501.
- [14] L. Black, C. Breen, J. Yarwood, K. Garbev, P. Stemmermann, B. Gasharova, Structural features of C–S–H (I) and its carbonation in air - a Raman spectroscopic study. Part II: carbonated phases, *J. Am. Ceram. Soc.* 90(3) (2007) 908-917.
- [15] M. Tlili, M.B. Amor, C. Gabrielli, S. Joiret, G. Maurin, P. Rousseau, Characterization of CaCO₃ hydrates by micro-Raman spectroscopy, *J. Raman. Spectrosc.* 33(1) (2002) 10-16.
- [16] J. Corvisier, F. Brunet, A. Fabbri, S. Bernard, N. Findling, G. Rimmelé, V. Barlet-Gouédard, O. Beyssac, B. Goffé, Raman mapping and numerical simulation of calcium carbonates distribution in experimentally carbonated Portland-cement cores, *Eur. J. Mineral.* 22(1) (2010) 63-74.
- [17] H. Rutt, J. Nicola, Raman spectra of carbonates of calcite structure, *J. Phys. C. Solid. State.* 7(24) (1974) 4522.
- [18] U. Wehrmeister, A. Soldati, D. Jacob, T. Häger, W. Hofmeister, Raman spectroscopy of synthetic, geological and biological vaterite: a Raman spectroscopic study, *J. Raman. Spectrosc.* 41(2) (2010) 193-201.
- [19] J. Ibáñez, L. Artús, R. Cuscó, Á. López, E. Menéndez, M.C. Andrade, Hydration and carbonation of monoclinic C₂S and C₃S studied by Raman spectroscopy, *J. Raman. Spectrosc.* 38(1) (2007) 61-67.
- [20] L. Black, C. Breen, J. Yarwood, J. Phipps, G. Maitland, In situ Raman analysis of hydrating C₃A and C₄AF pastes in presence and absence of sulphate, *Adv. Appl. Ceram.* 105(4) (2006) 209-216.
- [21] E. Knittle, W. Phillips, Q. Williams, An infrared and Raman spectroscopic study of gypsum at high pressures, *Phys. Chem. Miner.* 28(9) (2001) 630-640.

- [22] N. Buzgar, A. Buzatu, I.V. Sanislav, The Raman study on certain sulfates, *Analele. Științifice. Ale. Universității „Al. I. Cuza” Iași, Geologie* 55(1) (2009) 5-23.
- [23] A. Brough, A. Atkinson, Micro-Raman spectroscopy of thaumasite, *Cement. Concrete. Res.* 31(3) (2001) 421-424.
- [24] C. Wang, T.J. Vickers, J.B. Schlenoff, C.K. Mann, In situ monitoring of emulsion polymerization using fiber-optic Raman spectroscopy, *Appl. Spectrosc.* 46(11) (1992) 1729-1731.
- [25] M.G. Shim, B.C. Wilson, Development of an in vivo Raman spectroscopic system for diagnostic applications, *J. Raman. Spectrosc.* 28(2-3) (1997) 131-142.
- [26] J.T. Motz, M. Fitzmaurice, A. Miller, S.J. Gandhi, A.S. Haka, L.H. Galindo, R.R. Dasari, J.R. Kramer, M.S. Feld, In vivo Raman spectral pathology of human atherosclerosis and vulnerable plaque, *J. Biomed. Opt.* 11(2) (2006) 021003-021003-9.
- [27] M. Myrick, J. Kolis, E. Parsons, K. Chike, M. Lovelace, W. Scrivens, R. Holliday, M. Williams, In situ fiber-optic Raman spectroscopy of organic chemistry in a supercritical water reactor, *J. Raman. Spectrosc.* 25(1) (1994) 59-65.
- [28] A.M. Neville, *Properties of Concrete*, fifth ed., Prentice Hall, 2012.
- [29] B. Lagerblad, *Carbon dioxide uptake during concrete life cycle—state of the art*, Swedish Cement and Concrete Research Institute CBI, Stockholm (2005).
- [30] G. Groves, D. Rodway, I. Richardson, The carbonation of hardened cement pastes, *Adv. Cem. Res.* 3(11) (1990) 117-125.
- [31] A. Morandea, M. Thiery, P. Dangla, Investigation of the carbonation mechanism of CH and CSH in terms of kinetics, microstructure changes and moisture properties, *Cement. Concrete. Res.* 56 (2014) 153-170.
- [32] T.-W. Liao, H.-M. Chen, K.-Y. Shen, C.-H. Kuan, Pure, single crystal Ge nanodots formed using a sandwich structure via pulsed UV excimer laser annealing, *Nanotechnology.* 26(16) (2015) 165301.
- [33] C.-Y. Tsao, J.W. Weber, P. Campbell, P.I. Widenborg, D. Song, M.A. Green, Low-temperature growth of polycrystalline Ge thin film on glass by in situ deposition and ex situ solid-phase crystallization for photovoltaic applications, *Appl. Surf. Sci.* 255(15) (2009) 7028-7035.
- [34] E. Katainen, M. Elomaa, U.M. Laakkonen, E. Sippola, P. Niemelä, J. Suhonen, K. Järvinen, Quantification of the amphetamine content in seized street samples by Raman spectroscopy, *J. Forensic. Sci.* 52(1) (2007) 88-92.
- [35] ASTM E 579-04. Standard test method for limit of detection of fluorescence of quinine sulfate in solution, ASTM International. (2015).

- [36] J. Parker Jr, D. Feldman, M. Ashkin, Raman scattering by silicon and germanium, *Phys. Rev.* 155(3) (1967) 712.
- [37] T. Ogino, T. Suzuki, K. Sawada, The formation and transformation mechanism of calcium carbonate in water, *Geochim. Cosmochim. Ac.* 51(10) (1987) 2757-2767.
- [38] I. Richardson, J. Skibsted, L. Black, R.J. Kirkpatrick, Characterisation of cement hydrate phases by TEM, NMR and Raman spectroscopy, *Adv. Cem. Res.* 22(4) (2010) 233-248.